Supplementary Materials for

Ribosome-nascent chain interaction regulates N-terminal protein modification

Chien-I Yang, Jiwoo Kim, and Shu-ou Shan*

Division of Chemistry and Chemical Engineering, California Institute of Technology

1200 E. California Blvd, Pasadena, CA 91125

*Correspondence to: sshan@caltech.edu

This file includes:

Figures S1–S6

Supplementary References

Supplementary Figures

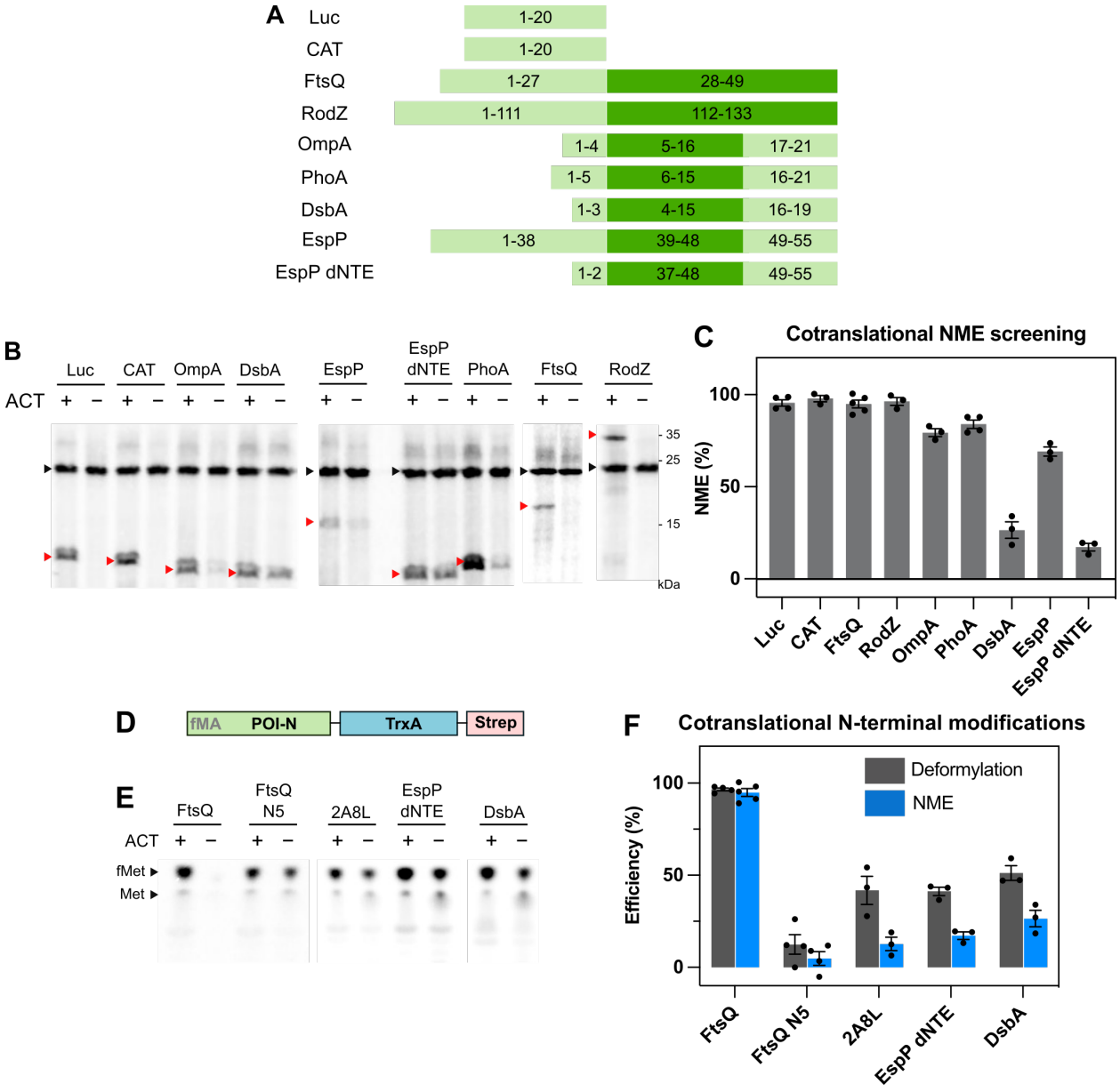

Figure S1: Cotranslational NME of model substrates in cell extracts. (A) Scheme of the POI-N used to screen for molecular features that regulate NME. Hydrophobic cores of the signal sequence or TMDs are colored in dark green. **(B)** Representative SDS/PAGE autoradiography for the cotranslational NME of the model substrates in (A). Red arrows indicate the substrate of interest, and black arrows indicate the loading control. Reactions with actinonin (ACT, 5µM) provided controls for the iMet signal from the substrates without NME. **(C)** Cotranslational NME efficiency of the indicated substrates, determined by the reduction of the iMet signal in the reactions without ACT relative to that in ACT-containing reactions. **(D)** Scheme of the model

substrates used to analyze the formylation state. A Strep tag was appended C-terminally to the reporter proteins depicted in Fig. 1B for immunoprecipitation. (**E**) Representative TLC analysis to quantify the fMet and Met on the substrates. The substrate proteins were translated in *E. coli* S30 lysates containing ^{35}S-Met, immunoprecipitated via the Strep tag, and digested by Proteinase K. fMet and Met were separated by TLC and quantified by autoradiography. **(F)** Summary of cotranslational deformylation and NME of the indicated substrates. Deformylation was determined by the reduction of the fMet signal in the "–ACT" samples relative to the "+ACT" samples, and NME was determined as in Figs. 1E, H and S1C. Values are reported as mean ± SEM with $n \geq 3$.

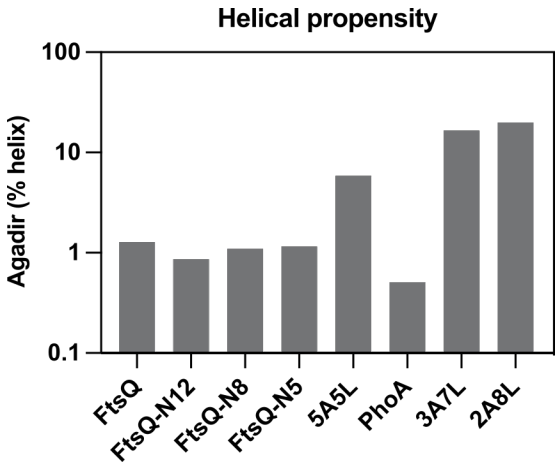

Figure S2: Secondary structure of the nascent chain is insufficient to explain the NME inhibition by an N-terminal membrane targeting signal. Prediction of helical propensity using the AGADIR algorithm (*1*) for the first 32 residues of FtsQ variants and first 34 residues of PhoA variants, corresponding to the exposed nascent chain sequence of the respective RNC in Fig. 2.

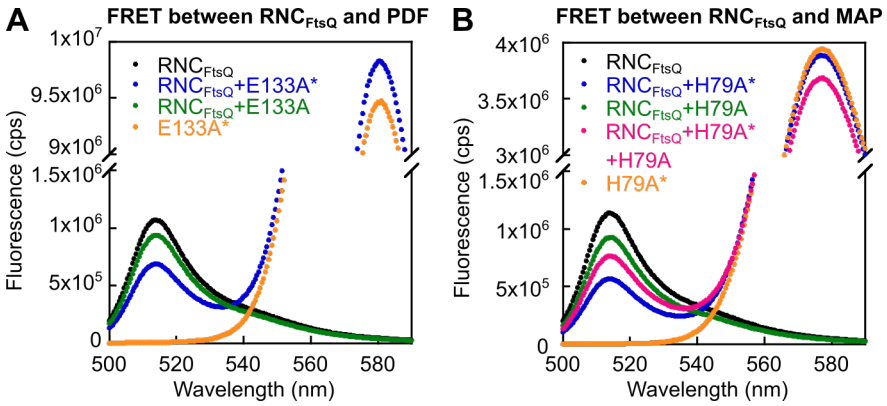

Figure S3: FRET assay to measure the binding between the ribosome and PDF or MAP. (**A**) Fluorescence emission spectra of 10 nM BDP-labeled RNC_{FtsQ} in the absence (*black*) and presence of 4 μM TMR-labeled *(blue*, indicated by '*') or unlabeled (*green*) PDF(E133A). Incubation of BDP-RNC_{FtsQ} with TMR-PDF(E133A) induced FRET, whereas unlabeled PDF(E133A) modestly reduced the donor fluorescence intensity due to environmental sensitivity. The fluorescence emission spectrum of 4 μM TMR-PDF(E133A) is shown in *orange*. (**B**) Fluorescence emission spectra of 10 nM BDP-RNC_{FtsQ} in the absence (*black*) or presence of 1 μM TMR-labeled (*blue*) or unlabeled (*green*) MAP(H79A). The FRET signal between BDP-RNC_{FtsQ} and TMR-MAP(H79A) can be chased by unlabeled MAP(H79A) (2.5 μM, *magenta*). The fluorescence emission spectrum of 1 μM TMR-MAP(H79A) is shown in *orange*.

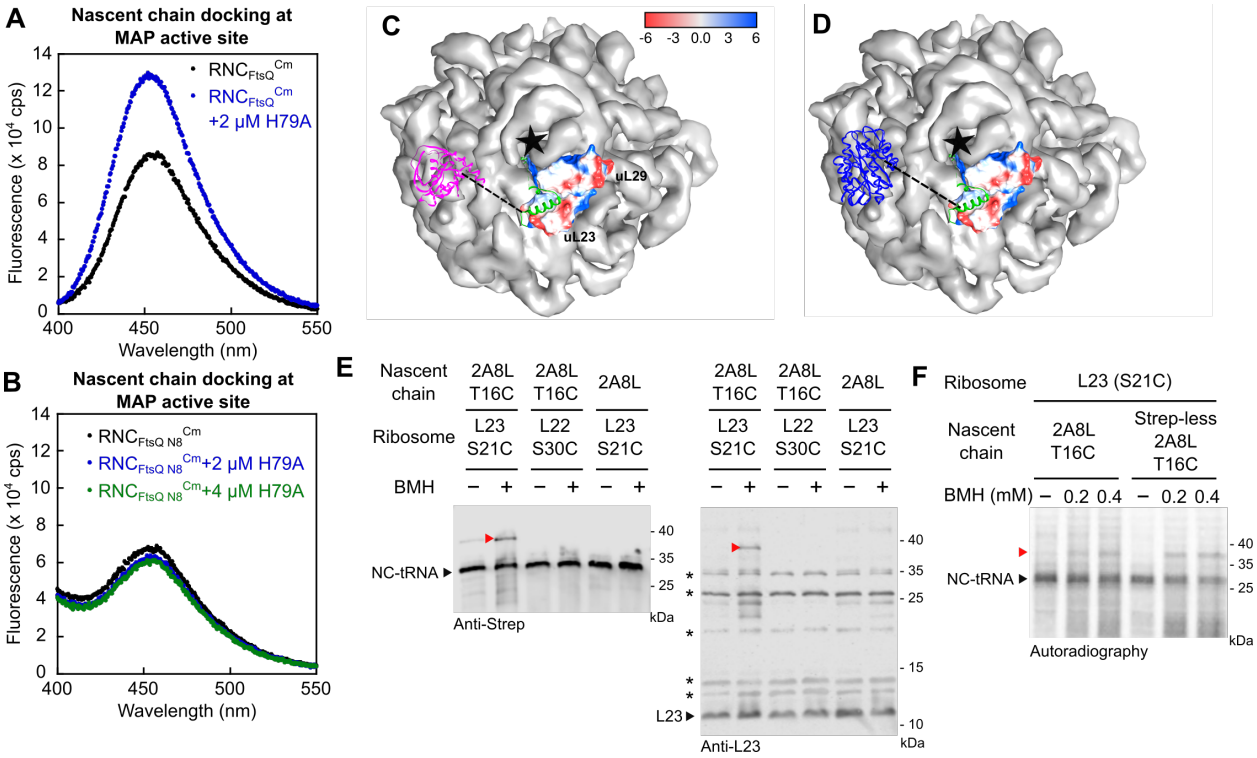

Figure S4: Interaction with the ribosomal surface prevents the nascent chain from accessing PDF and MAP. (A) and **(B)** Fluorescence assay to report on the local environment of the nascent chain N-terminus. L-(7-hydroxycoumarin-4-yl)ethylglycine (Cm) was incorporated at the fifth position of the FtsQ (A) and FtsQ-N8 (B) nascent chains during translation. Purified RNC was incubated with the indicated amount of MAP(H79A). The enhancement in the fluorescence intensity of RNC_{FtsQ}^{Cm} upon the addition of MAP(H79A) (A) reports on docking of the nascent chain N-terminus at the MAP active site (*2*); this fluorescence change is not observed with $RNC_{FtsQ\ N8}^{Cm}$ in (B). **(C)** and **(D)** Models of PDF (C, *magenta*) or MAP (D, *blue*) bound to an RNC with an emerging TMD (*green*), viewed from the ribosome tunnel exit (star). The models were generated by overlaying the 70S structures of an RNC bearing the nascent chain of a membrane protein RodZ (PDB-6S0K) and the PDF-bound (EMD-9750) or MAP-bound (EMD-9752) ribosome using UCSF Chimera. The Coulombic surface potential of uL23 and uL29 were generated using Chimera, and colored as indicated in units of kcal·mol^{-1}·e^{-1}at 298K, where e denotes the charge of a proton. The distances from the N-terminus of the TMD to the active site of PDF and MAP (dashed lines) are 48 Å and 54 Å, respectively. **(E)** Representative western blot

for the crosslink between RNC_{2A8L} and uL23. RNC_{2A8L} variants with or without the indicated cysteine mutations were incubated in the presence or absence of 0.4 mM bismaleimidohexane (BMH). Crosslinked product (red arrows) was detected with anti-Strep (for nascent chain) and anti-L23 antibodies. Asterisks, non-specific bands detected by the anti-uL23 antibody. **(F)** Representative SDS/PAGE and autoradiograph of the crosslink between RNC_{2A8L} and uL23 for nascent chains with or without the N-terminal 3X Strep tag. RNC_{2A8L} was generated by *in vitro* translation in S30 extract in the presence of ^{35}S-Met, purified via sucrose gradient fractionation, incubated with indicated amount of BMH, and analyzed by autoradiography. The crosslinked product (red arrow) was independent of the presence of the Strep tag.

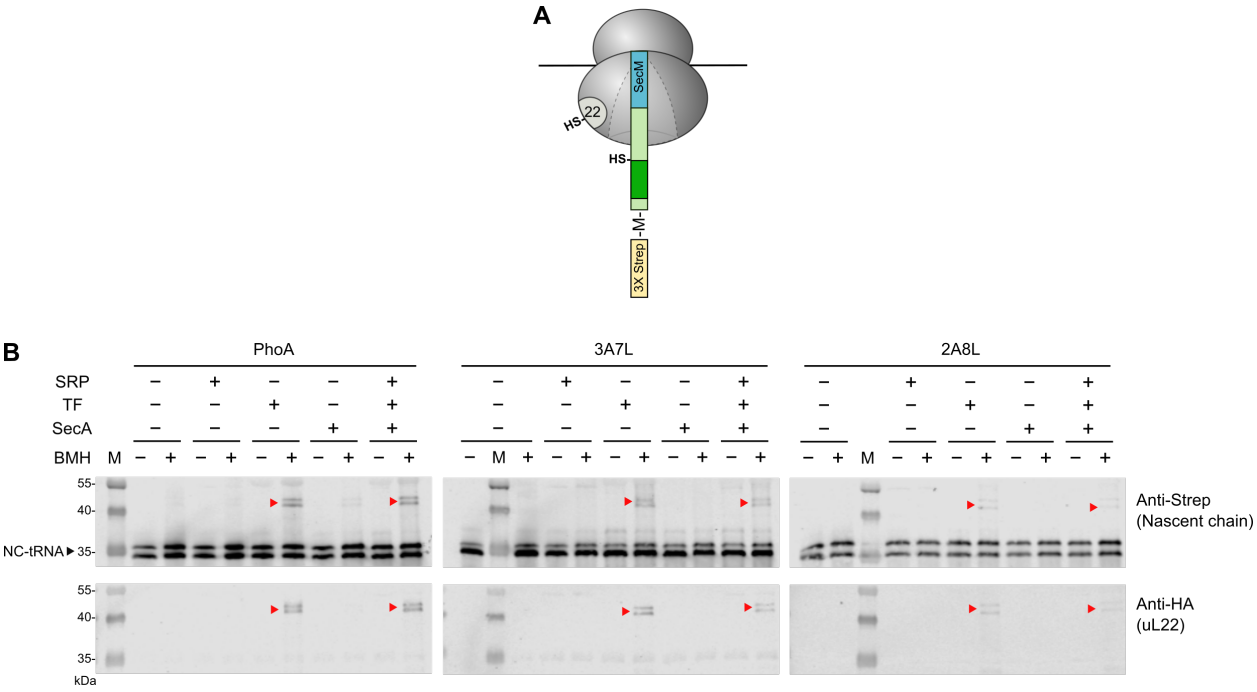

Figure S5: TF reorients the nascent chains. (A) Scheme of the RNCs used to detect the proximity of the nascent chains to uL22. The mutation S30C and a C-terminal HA tag were genetically introduced into uL22, and a cysteine was placed near the signal sequence (dark green) of the model substrates, as detailed in *Methods*. **(B)** Crosslinking between the indicated nascent chains and uL22. The RNCs (500 nM) were incubated with or without 1.6 mM 1,4-bismaleimidohexane (BMH) in the absence or presence of 500 nM SRP, 10 µM TF or 1 µM SecA, and analyzed by Western blot analysis using anti-Strep (for nascent chain) and anti-HA (for uL22) antibodies. The crosslinked products between the nascent chain and uL22 (red arrows) were only detected in the presence of TF. M: molecular weight marker.

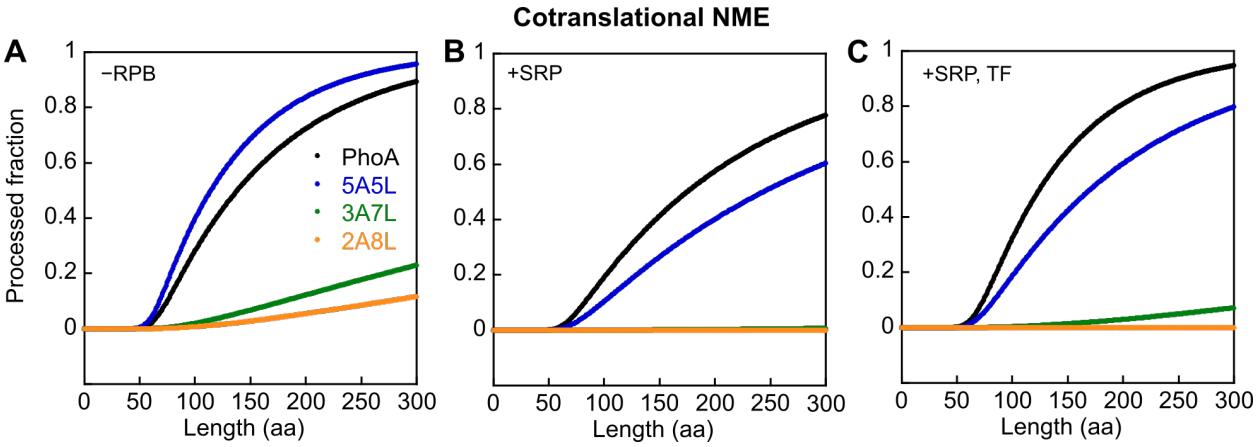

Figure S6: Kinetic simulation of the cotranslational NME of PhoA variants. The cumulative fraction of the indicated model nascent chains successfully processed by both PDF and MAP during ongoing translation were calculated using the numerical integration method (*2*) in the absence of RPBs (A), in the presence of SRP (B), and with both SRP and TF present (C). The calculations were carried out under the following assumptions: (i) NME initiates after 45 aa of the nascent chain are translated. (ii) The k_{cat}/K_m values of the PDF and MAP reactions increase linearly to the experimentally measured values in Figs. 4B and 4D as the nascent chain elongates from 45 to 69 aa, and remain constant thereafter.

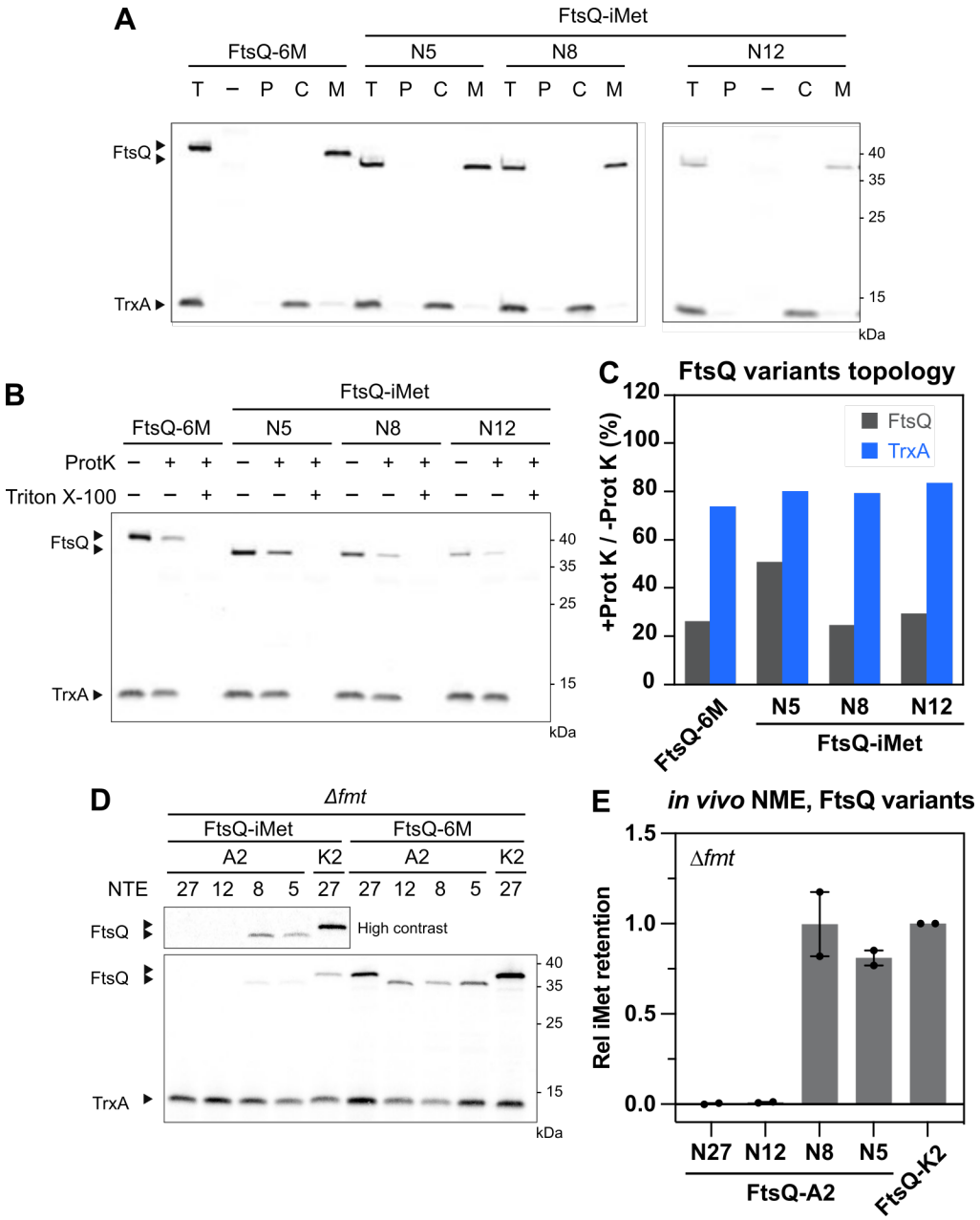

Figure S7: Additional data for *in vivo* NME of FtsQ variants. (A) Cellular localization of the indicated FtsQ variants. Cells expressing the model substrates and the control protein TrxA from the constructs described in Fig. 5A were collected, lysed and fractionated as described in *Methods*. The sub-cellular fractions were analyzed by Western blotting with anti-FLAG antibody. T: total lysate; P: periplasm; C: cytoplasm; M: membrane. **(B)** Topology of the indicated FtsQ variants. Spheroplasts were prepared from cells expressing the model substrates, treated with proteinase K (ProtK) in the presence or absence of Triton X-100, and analyzed by Western blotting with anti-FLAG antibody. **(C)** Quantification of the remaining protein signals after the ProtK treatment in

(B). The C-terminal FLAG tag on cytosolic TrxA was resistant to ProtK, whereas those on FtsQ-*6M*, FtsQ N12-*iMet* and FtsQ N8-*iMet* were susceptible to ProtK cleavage, consistent with the N-in-C-out topology**. (D)** *In vivo* NME of the FtsQ NTE truncation variants in the Δ*fmt* strain (KPS73), measured as described in Fig. 5B. **(E)** Quantification of the data in (D) and replicates. Values are normalized to FtsQ-K2 and reported as mean ± SEM, with n = 2 biological replicates.

Supplementary References

1. V. Muñoz, L. Serrano, Elucidating the Folding Problem of Helical Peptides using Empirical Parameters. II†. Helix Macrodipole Effects and Rational Modification of the Helical Content of Natural Peptides. *Journal of Molecular Biology*. **245**, 275–296 (1995).

2. C.-I. Yang, H.-H. Hsieh, S. Shan, Timing and specificity of cotranslational nascent protein modification in bacteria. *Proc. Natl. Acad. Sci. U.S.A.* **116**, 23050–23060 (2019).